

The $\alpha + \varepsilon$ Two-Phase Equilibrium in the Fe-N-C System: Experimental Investigations and Thermodynamic Calculations



HOLGER GÖHRING, ANDREAS LEINEWEBER, and ERIC JAN MITTEMEIJER

The present work is dedicated to investigating the occurrence of the $\alpha + \varepsilon$ equilibrium at temperatures typically applied for nitrocarburizing treatments. To this end, pearlitic Fe-C specimens were treated between 823 K and 863 K (550 °C and 590 °C) in gaseous nitriding and gaseous nitrocarburizing atmospheres, allowing control of the chemical potentials of N and C. Subsequently, the resulting compound-layer microstructures were investigated using light microscopy and X-ray diffraction. Thermodynamic calculations, adopting several models for the Fe-N-C system from the literature, were performed, showing significantly different predictions for both the sequence of the invariant reactions and their temperatures. Comparison of the experimental data and the theoretical calculations led to the conclusion that none of the models from the literature is able to realistically describe the experimentally observed constitution in the Fe-N-C system in the considered temperature range. Values/value ranges for the temperatures of the invariant reactions were obtained.

DOI: 10.1007/s11661-016-3605-5

© The Author(s) 2016. This article is published with open access at Springerlink.com

I. INTRODUCTION

A. Equilibrium, Metastable Equilibrium, and Local Equilibrium

PHASE equilibria of the Fe-N-C system have been studied extensively in the past. The first attempt to determine an isothermal section of the phase diagram [at 723 K (450 °C) and at 1×10^5 Pa] was performed by Jack.^[1] Probably, the most influential study on solid-state equilibria in this ternary system was performed by Naumann and Langenscheid.^[2] They presented isothermal sections of the Fe-N-C phase diagram at 1×10^5 Pa between 773 K and 973 K (500 °C to 700 °C). This work was the main reference to the later reviews in References 3 through 5.

For an overview of the relevant phases in the system Fe-N-C, indicating crystallographic and compositional characteristics, as assembled from References 6 and 7,

see Table I. These phases have in common that at 1×10^5 Pa they are metastable with respect to decomposition into α -Fe or γ -Fe (with low interstitial content), graphite, and nitrogen gas. They can be stabilized *at the surface* of specimens by imposing specific chemical potentials of N and C at the surface of the specimen, *e.g.*, by gaseous nitriding/nitrocarburizing. Thus, in the sequel, with the term *equilibrium*, always a metastable equilibrium is meant. Note that similar remarks hold for the established Fe-N^[8] and Fe-C^[9] binary phase diagrams.^[7,10,11]

As in the present work, the experimental data for the phase constitution of the Fe-N-C system is usually obtained from gas nitrided or gas nitrocarburized specimens consisting originally of pure Fe or of Fe-N or Fe-C alloys. During these thermochemical surface treatment processes, and as a consequence of specific imposed chemical potentials of N and C in the gas phase, (further) N and C can be taken up into the specimen from the gas atmosphere. At intermediate stages, a diffusion zone and, if sufficiently high chemical potentials of N and C in the gas atmosphere prevail, as in the present work, a compound layer on top develop.^[7,10] Thus, N and C concentration gradients occur in both the compound layer and the diffusion zone. The corresponding microstructures do not represent the true equilibrium state for the entire specimen, as prescribed by its gross composition, the temperature, and the pressure. However, it can be assumed^[12] that at each depth below the surface local equilibrium with respect to the local, lateral gross composition, the temperature, and the pressure is established, especially at the interfaces between the Fe-N-C solid-solution phases, *i.e.*, the sublayer boundaries and the interface with the substrate. The phase constitution as a function

HOLGER GÖHRING, Ph.D. Student is with the Max Planck Institute for Intelligent Systems (formerly Max Planck Institute for Metals Research), Heisenbergstraße 3, 70569 Stuttgart, Germany. Contact email: h.goehring@is.mpg.de ANDREAS LEINEWEBER, formerly Research Scientist with the Max Planck Institute for Intelligent Systems, is now Professor with the Institute of Materials Science, TU Bergakademie Freiberg, Gustav-Zeuner-Str. 5, 09599 Freiberg. ERIC JAN MITTEMEIJER, Director, is with the Max Planck Institute for Intelligent Systems, and also Professor with the Institute for Materials Science, University of Stuttgart, Stuttgart, Germany.

Manuscript submitted January 22, 2016.

Article published online July 13, 2016

Table I. Crystal Structures and (Ranges of) N and C Content, x_N and x_C , of Phases Relevant for the Present Work According to Refs. [6] and [7]

Phase	Space Group	Structure Description	x_N /at. pct	x_C /at. pct
α -Fe[N,C]	$Im\bar{3}m$	bcc Fe lattice, N and C on octahedral sites	<0.4	<0.1
γ -Fe[N,C]	$Fm\bar{3}m$	fcc Fe lattice, N and C on octahedral sites	<10.3	<9.1
γ' -Fe ₄ N _{1-x}	$Pm\bar{3}m$	fcc Fe lattice, N ordered on octahedral sites	19.4 to 20	<0.7
ε -Fe ₃ (N,C) _{1+x}	$P6_322$	hcp Fe lattice, N and C ordered on octahedral sites	15 to 33	<8
θ -Fe ₃ C	$Pnma$	orthorhombic, C in trigonal prisms of Fe	≈ 0	25

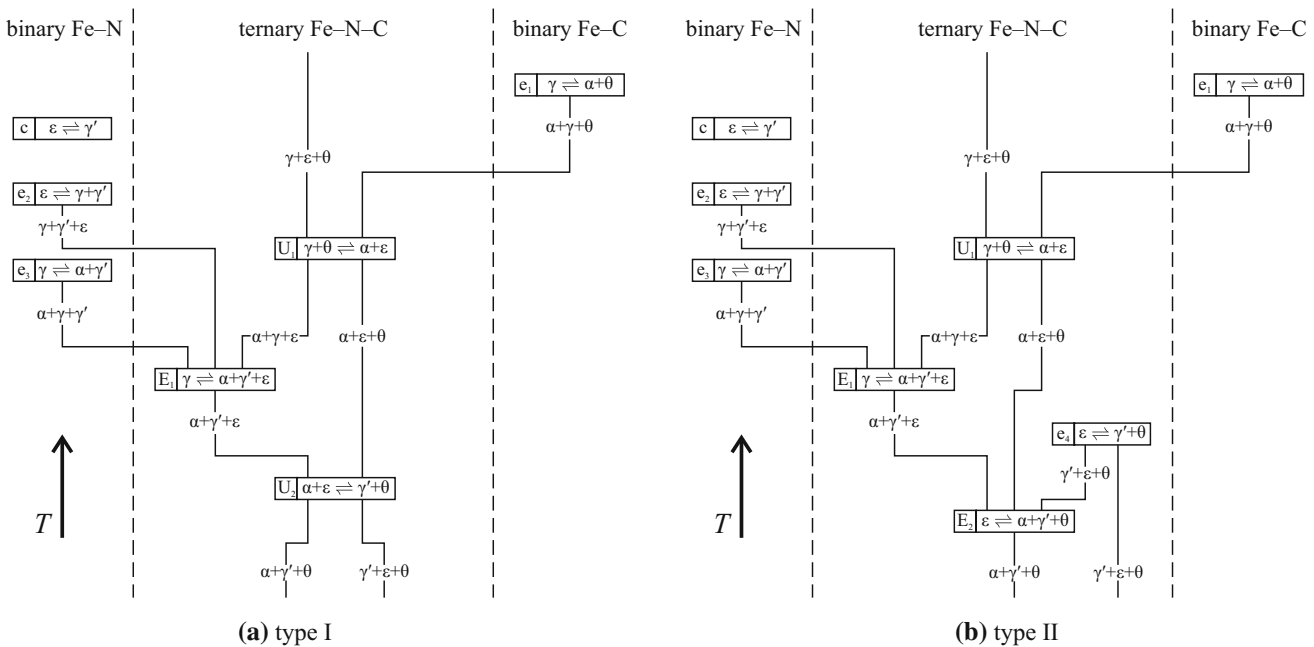


Fig. 1—Schematic Scheil reaction schemes showing the two possibilities for the (sequence of) invariant reaction(s) leading from the $\alpha + \varepsilon$ equilibrium to the $\gamma' + \theta$ equilibrium upon cooling, cf. Fig. 2. Both Scheil reaction schemes comprise the c, e₁, e₂, e₃, E₁, and U₁ invariant reactions. The invariant reaction U₂ is unique to the type I Scheil reaction scheme (a), whereas it is replaced by the reactions e₄ and E₂ in the type II Scheil reaction scheme (b).

of depth can be predicted using the concept of diffusion paths:^[13–16] the evolution of the (laterally averaged) composition as a function of depth allows to plot these composition data in a phase diagram at the temperature (and pressure) concerned, which data together constitute the diffusion path. If local equilibrium at each point of the diffusion path and thus at each depth in the specimen *separately* prevails, the sequence of the phases developing within the compound layer and the diffusion path can be related with the corresponding phase diagram,^[13–15] e.g., see Reference 12.

B. Constitution and Invariant Reactions in the Fe-N-C System

At least at typical nitriding/nitrocarburizing temperatures, an $\alpha + \varepsilon$ equilibrium does not exist in the binary Fe-N phase diagram. However, in the additional presence of C, α/ε phase boundaries are often observed,

indicating the presence of a local $\alpha + \varepsilon$ equilibrium. Considering the experimental results presented in the “old” References 17 and 2, it is possible to deduce in retrospect that ε can occur in direct contact with α . In Reference 17, a micrograph (their Figure 3) was given, showing ε forming a network along α grain boundaries after prolonged nitrocarburizing of Fe at 843 K (570 °C). In Reference 2, the conclusion that an $\alpha + \varepsilon$ equilibrium does not occur is based on a single specimen treated at 853 K (580 °C), interpreted to contain γ . All other experimental data presented in Reference 2 at the temperatures of 873 K (600 °C) and below can be compatible with the occurrence of an $\alpha + \varepsilon$ equilibrium. In both references, a possible occurrence of an $\alpha + \varepsilon$ equilibrium was not recognized.

In later works,^[12,18–32] microstructures with α and ε in direct contact were frequently found and recognized as such. On this basis, at present an equilibrium of α and ε is accepted and included in all recent thermodynamic

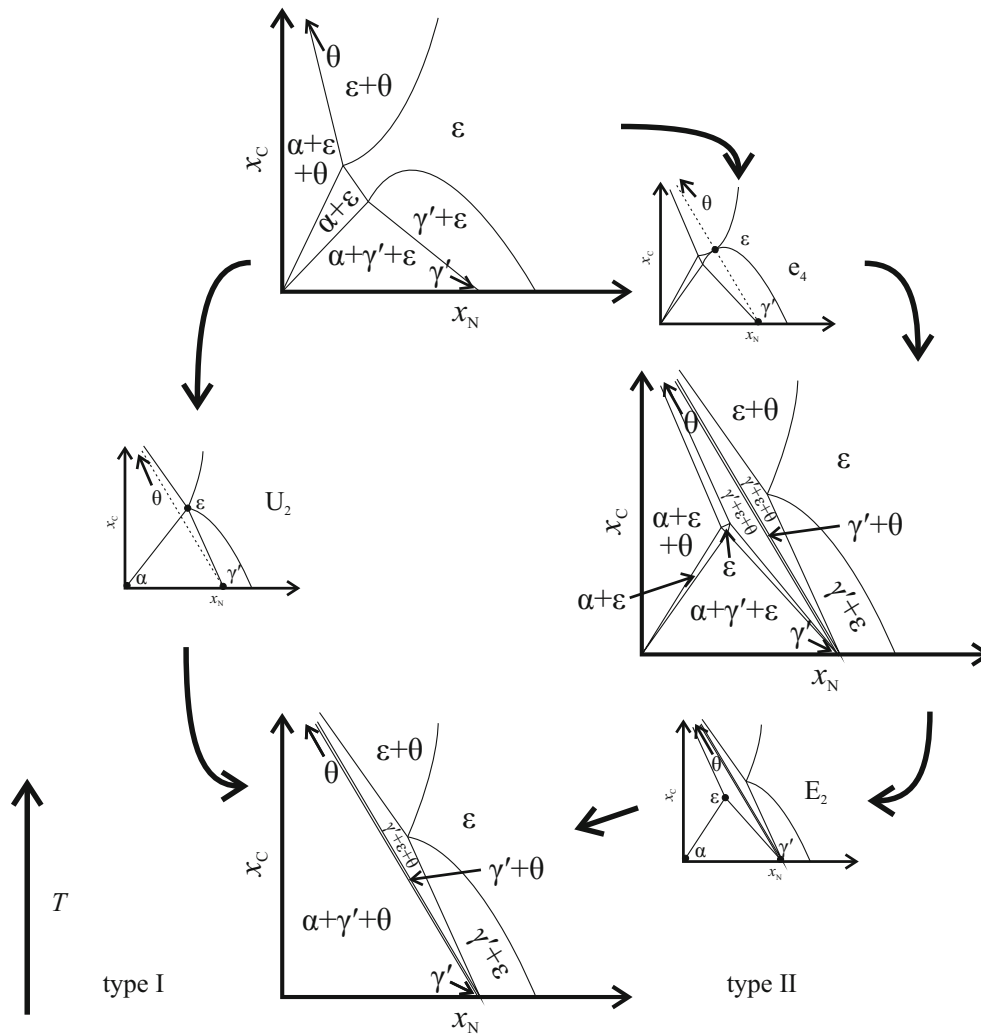


Fig. 2—Schematic isothermal sections of the Fe-N-C phase diagram illustrating the two possibilities for the (sequence of) invariant reaction(s) in the system Fe-N-C leading to the replacement of the $\alpha + \epsilon$ equilibrium by the $\gamma' + \theta$ equilibrium upon cooling. At the temperatures of the invariant reactions e_4 , E_2 , and U_2 , the compositions of the phases in equilibrium (e_4 : three phases; E_2 and U_2 : four phases; except the θ phase) have been indicated by solid dots. At these temperatures, two-phase equilibria existing above and below the invariant temperature have been indicated by solid and dashed lines, respectively. Left part: in the type I sequence of invariant reactions, the $\alpha + \epsilon$ equilibrium is directly replaced by the $\gamma' + \theta$ equilibrium via the transitional reaction U_2 , $\alpha + \epsilon \rightleftharpoons \gamma' + \theta$. Right part: in the type II sequence of invariant reactions, upon cooling, the $\gamma' + \theta$ equilibrium is introduced via the pseudo-binary eutectoid reaction e_4 , $\epsilon \rightleftharpoons \gamma' + \theta$, dividing the ϵ single-phase field into two separate ϵ single-phase fields; see the isothermal section of the phase diagram in the middle right part of the figure. The second ϵ single-phase field at low interstitial content vanishes via the ternary eutectoid reaction E_2 , $\epsilon \rightleftharpoons \alpha + \gamma' + \theta$.

models of the Fe-N-C system.^[33–38] The $\alpha + \epsilon$ equilibrium is of pronounced relevance for nitrocarburizing of ferritic steels: by appropriate choice of the process parameters, it is possible to obtain a single-phase ϵ layer in contact with the substrate, which corresponds to improved anticorrosion, wear, and tribological properties.^[10]

The sequence of invariant reactions in the Fe-N-C system possibly met upon cooling at $T \leq 1000$ K (727 °C) can be visualized in a Scheil reaction scheme^[39–41] as shown in Figure 1. From the binary systems, the congruent transition c [Fe-N, $\epsilon \rightleftharpoons \gamma'$, 953 K (677 °C)^[8]] as well as the well-established eutectoid reactions e_1 [Fe-C, $\gamma \rightleftharpoons \alpha + \theta$, 1000 K (727 °C)^[9]], e_2 [Fe-N, $\epsilon \rightleftharpoons \gamma + \gamma'$, 923 K (650 °C)^[8]], and e_3 [Fe-N, $\gamma \rightleftharpoons \alpha + \gamma'$, 865 K (592 °C)^[8]] are inherited, giving rise to two-phase ($\gamma' + \epsilon$) and three-phase ($\alpha + \gamma + \theta$, $\gamma + \gamma' + \epsilon$, $\alpha + \gamma + \gamma'$; in that order upon

decreasing temperature) fields in the ternary system. In the ternary system, at high temperatures, an equilibrium between γ and θ exists, vanishing upon cooling and being replaced by the $\alpha + \epsilon$ equilibrium via the U_1 invariant reaction, $\gamma + \theta \rightleftharpoons \alpha + \epsilon$. Upon further cooling, the γ phase vanishes via the ternary eutectoid reaction E_1 , $\gamma \rightleftharpoons \alpha + \gamma' + \epsilon$. Both reactions (U_1 and E_1) involving the γ phase have been investigated recently in an experimental study of the Fe-N-C system^{[32]*}; the temperature

*In Reference 32, the numbering of reactions U_1 and U_2 has been inverted.

of the invariant reaction U_1 , as first determined in Reference 32 to occur between 868 K and 873 K (595 °C to 600 °C), was confirmed in Reference 42.

At even lower temperatures, the $\alpha + \varepsilon$ equilibrium is replaced by an equilibrium between γ' and θ . This can occur *via* the invariant reaction U_2 . This sequence of invariant reactions is illustrated in the Scheil reaction scheme in Figure 1(a) and in the left part of Figure 2. However, in principle, this is only *one* of the *two* possibilities to realize the transition from the $\alpha + \varepsilon$ equilibrium at higher temperature to the $\gamma' + \theta$ equilibrium at lower temperature, assuming that ε is the only phase existing in this temperature range with a considerable homogeneity range and that γ does not participate in the considered invariant reactions. The second possibility is shown in the Scheil reaction scheme in Figure 1(b), which can be discussed considering the right part of Figure 2. Upon cooling, the ε single-phase field is divided into two separate ε single-phase fields at the temperature of the pseudo-binary eutectoid reaction^[43] e_4 , $\varepsilon \rightleftharpoons \gamma' + \theta$, giving rise to the $\gamma' + \theta$ two-phase field upon continued cooling. The ε single-phase field at relatively low interstitial content (see middle right part of Figure 2), with the $\alpha + \varepsilon$ two-phase field, vanishes at lower temperature *via* the ternary eutectoid reaction E_2 , $\varepsilon \rightleftharpoons \alpha + \gamma' + \theta$. In the following, the first series of invariant reactions is referred to as type I and the latter one as type II.

In Reference 30, pure α -Fe specimens nitrocarburized at 823 K (550 °C), resulting in a $\gamma'/\gamma' + \theta$ layer on top of the substrate, were subsequently annealed at higher temperatures (in steps of 10 K), leading to a microstructure with α in direct contact with ε at 843 K (570 °C) and above. Also, α -Fe specimens nitrocarburized at 853 K (580 °C), resulting in a γ'/ε layer on top of the substrate, were subsequently annealed at lower temperatures (in steps of 10 K). Therefore, the $\alpha + \varepsilon$ equilibrium vanished at the annealing temperatures of 833 K (560 °C) and below. It was concluded that the transitional reaction $\alpha + \varepsilon \rightleftharpoons \gamma' + \theta$ occurs at a single temperature between 833 K and 843 K (560 °C to 570 °C) (reaction U_2 in Figures 1(a) and 2).

The present work is a follow-up and distinct extension of the work performed in Reference 30. Deliberately, significantly different types of microstructures distinctly different from those produced in Reference 30 were generated in the current project by nitriding and nitrocarburizing of pearlitic Fe-C alloys. The experimentally obtained results were compared to predictions from several existing thermodynamic models of the system Fe-N-C.^[33–38] Since the present work focuses on the $\alpha + \varepsilon$ equilibrium, the following data are of paramount interest: (i) at which temperature the $\alpha + \varepsilon$ equilibrium disappears and the $\gamma' + \theta$ equilibrium appears upon cooling (reaction U_2 or e_4 and E_2), and (ii) which sequence of invariant reactions (type I or type II) occurs upon cooling establishing the disappearance of the $\alpha + \varepsilon$ equilibrium and the appearance of the $\gamma' + \theta$ equilibrium. The temperature at which the $\alpha + \varepsilon$ equilibrium disappears can be determined by choosing conditions that lead to unambiguous microstructures proving the presence of the $\gamma' + \theta$ equilibrium below and the $\alpha + \varepsilon$ equilibrium above that temperature. Distinguishing the occurrence in reality of the sequence of invariant reactions

of type I from the sequence of invariant reactions of type II is difficult: in principle, all microstructures featuring an $\alpha + \varepsilon$ equilibrium are compatible with phase diagrams corresponding to the sequence of invariant reactions of type I above the temperature of the U_2 reaction, but also with phase diagrams corresponding to the sequence of invariant reactions of type II above the temperature of the E_2 reaction. The sequence of invariant reactions of type II can only be proven by the presence of both the $\alpha + \varepsilon$ equilibrium and the $\gamma' + \theta$ equilibrium at a range of temperatures, *i.e.*, between the temperatures of the e_4 and E_2 invariant reactions (see the middle right part of Figure 2), whereas according to the sequence of invariant reactions of type I this can only occur at one temperature (the temperature of the U_2 invariant reaction). With this in mind, the experiments performed in the present work had been designed.

II. THERMODYNAMIC CONSIDERATIONS

A. Thermodynamics of Interstitial Solid Solutions

The thermodynamics of the system Fe-N-C can be described by modeling the temperature and composition dependence of the Gibbs energy of each phase, *e.g.*, using the Calphad approach.^[44] In the past, this has been performed several times.^[33–38,45] In the following, the Gibbs energy models employed in these works^[33–38,45] are introduced.

The phases in the system Fe-N-C can be regarded as interstitial solid solutions of N and C in an Fe lattice. Thus, the Gibbs energy of one formula unit of such a phase ϕ , $Fe_a(C,N,Va)_c$, where Va denotes a vacant site on the interstitial sublattice, and with integers a and c , the ratio of which is determined by the crystal structure, can be described as (Hillert–Staffanson approach, also called compound-energy formalism^[46–48])

$$G_m^\phi = y_C^\phi \circ G_{Fe:C}^\phi + y_N^\phi \circ G_{Fe:N}^\phi + y_{Va}^\phi \circ G_{Fe:Va}^\phi + cRT(y_C^\phi \ln y_C^\phi + y_N^\phi \ln y_N^\phi + y_{Va}^\phi \ln y_{Va}^\phi) + G^{\phi,ex} + G^{\phi,mag} \quad [1]$$

with y_C^ϕ , y_N^ϕ and y_{Va}^ϕ as the site fractions of C, N, and Va, respectively, on the interstitial sublattice, $\circ G_{Fe:C}^\phi$, $\circ G_{Fe:N}^\phi$, and $\circ G_{Fe:Va}^\phi$ as the standard Gibbs energy of the real or hypothetical compounds (“end members”) Fe_aC_c , Fe_aN_c , and Fe_aVa_c , respectively, with the crystal structure of the phase ϕ and in the state of no magnetic order (with Fe:C, Fe:N, and Fe:Va denoting that the second, interstitial sublattice is fully occupied by C, N, and Va, respectively), $G^{\phi,ex}$ as the excess Gibbs energy, and $G^{\phi,mag}$ as the magnetic contribution.

The excess Gibbs energy can be modeled as

$$G^{\phi,ex} = y_C^\phi y_N^\phi L_{Fe:C,N}^\phi + y_C^\phi y_{Va}^\phi L_{Fe:C,Va}^\phi + y_N^\phi y_{Va}^\phi L_{Fe:N,Va}^\phi + y_C^\phi y_N^\phi y_{Va}^\phi L_{Fe:C,N,Va}^\phi \quad [2]$$

Table II. Temperatures in K (°C in Parentheses) of the Invariant Reactions (cf. Fig. 1) as Predicted by Models for the System Fe-N-C in the Literature and as Experimentally Determined in Ref. [32] (Invariant Reactions c, e₂, E₁, and U₁), Ref. [61] (Invariant Reaction e₃), and in the Present Work (Invariant Reaction U₂ for Type I Model, Invariant Reactions e₄ and E₂ for Type II Model)

Type	Slycke <i>et al.</i> ^[33]	Kunze ^[34]	Du/Hillert ^[35]	Du ^[36]	Kunze ^[37]	SGTE ^[38]	Experimental Data	
	I	II	I	I	II	I	I/II	
c	964 (691)	954 (681) ^(*)	970 (697)	971 (698)	955 (682) ^(*)	972 (699)	938 to 948 (665 to 675) [32]	
e ₁	1000 (727)	1000 (727)	1000 (727)	1000 (727)	1000 (727)	1000 (727)	—	
e ₂	922 (649) [*]	921 (648)	923 (650) [*]	923 (650) [*]	923 (650) [*]	917 (644)	923 to 925 (650 to 652) [32]	
e ₃	865 (592) [*]	868 (595) [*]	863 (590) [*]	863 (590) [*]	867 (594) [*]	864 (591) [*]	866 (593) ^a [61]	
e ₄		832 (559)			833 (560)		840 to 844 (567 to 571) this work	
E ₁	858 (585) [*]	858 (585) [*]	849 (581)	859 (586) [*]	857 (584) [*]	848 (575)	853 to 863 (580 to 590) [32]	
E ₂		825 (552)			825 (552)		840 to 844 (567 to 571) this work	
U ₁	863 (590)	954 (681)	853 (580)	867 (594) [*]	952 (679)	849 (576)	868 to 873 (595 to 600) [32]	
U ₂	824 (551)		821 (548)	783 (510)		841 (568) [*]	842 ± 2 (569 ± 2) this work	

Matches between the calculated and experimentally determined data are marked with an asterisk.

^aNo error margin given.

with the binary interaction parameters $L_{\text{Fe:C,N}}^{\phi}$, $L_{\text{Fe:C,Va}}^{\phi}$, and $L_{\text{Fe:N,Va}}^{\phi}$ and the ternary interaction parameter $L_{\text{Fe:C,N,Va}}^{\phi}$ ^{**}. Therefore, the binary interaction param-

^{**}In References 34 and 37, the model for the ϵ phase has been formulated in the compound-energy formalism. Afterwards, the equations for the chemical potentials of Fe, N, and C have been simplified. In order to correctly reformulate the resulting model in the compound-energy formalism as done in the current work, a ternary interaction parameter is needed.

ters can be expressed by a concentration-dependent Redlich–Kister series,^[49] *e.g.*, for $L_{\text{Fe:C,N}}^{\phi}$:

$$L_{\text{Fe:C,N}}^{\phi} = \sum_{k=0}^n k L_{\text{Fe:C,N}}^{\phi} (y_{\text{C}} - y_{\text{N}})^k. \quad [3]$$

For the ternary interaction parameter $L_{\text{Fe:C,N,Va}}^{\phi}$ a concentration dependence can also be introduced, which was, however, not applied in the cited thermodynamic models.^[33–38,45]

B. Comparison of Thermodynamic Descriptions: Invariant Reactions

The previous thermodynamic descriptions of the system Fe-N-C^[33–38,45] provide values for the parameters as defined by Eqs. [1] through [3] obtained by fitting the model to experimental data. The differences between the various descriptions^[33–38,45] boil down to different values (including the temperature dependence) adopted for some of the model parameters (*e.g.*, equating them to the values of the corresponding parameters for the binary systems; for Fe-N from References 50 through 53; for Fe-C from References 50 and 54) and different numbers of to-be-fitted parameters.

The first complete thermodynamic description of the system Fe-N-C^[45] has been assembled from the existing parameters for the binary and ternary systems from the

literature^[50,55,56] together with the estimated parameters for the ternary system. This model was not intended as a standalone model for the system Fe-N-C, but rather as only a building stone for a thermodynamic model of the quaternary Fe-Cr-N-C system. Furthermore, this study was focused only at a single temperature of 1273 K (1000 °C), *i.e.*, far out of the range of temperatures relevant for nitrocarburizing [say, 773 K to 923 K (500 °C to 650 °C)]. It is therefore perhaps not surprising that, adopting this model, a sequence of invariant reactions is predicted that differs pronouncedly from (especially recent) experimental data and from predictions obtained from more recent models.^[33–38] Thus, this model is not further considered in the present work.

Using values for the parameters of the Gibbs energy equations, *i.e.*, the Gibbs energies of the end members and the interaction parameters as defined by Eqs. [1] through [3], given in each of the References 33 through 38, isothermal sections were calculated using ThermoCalc^[57] in the present work for each model^[33–38] at different temperatures in order to determine the sequence of invariant reactions. Subsequently, the temperatures of the invariant reactions were calculated by setting the amounts (and not the compositions) of the three or four phases participating in each of the invariant equilibria to a fixed value. It was found that the models from References 33, 35, 36 and 38[†] lead to a

[†]Another series of invariant reactions than stated here was shown in the Scheil reaction scheme given in Reference 38, with the reactions U₁ and E₁ being degenerated, *i.e.*, occurring at exactly the same temperature. However, using the actual Gibbs energy equations of Reference 38 leads to the type I series of invariant reactions, albeit the calculated temperatures of the reactions U₁ and E₁ lie within 1 K.

type I series of invariant reactions, and the models from References 34 and 37 lead to a type II series of invariant reactions (cf. Section I–B and Figures 1 and 2). The temperatures of the invariant reactions as calculated using the models of References 33 through 38 have been

Table III. Temperatures, Treatment Times, Composition of Gas Atmospheres Applied for Nitrocarburizing (Series NC) and Nitriding (Series N) Treatments, and Resulting N Activity (Reference State N₂ Gas at 1×10⁵Pa) and C Activity (Reference State Graphite at 1×10⁵Pa) as Calculated Using the Data from Ref. [62]. $\phi_i = p_i/^\circ p$, with p_i as the Partial Pressure of Component i and $^\circ p = 1 \times 10^5 \text{ Pa}$

Series	$T / \text{K} (^\circ\text{C})$	t / h	ϕ_{NH_3}	ϕ_{H_2}	ϕ_{CO}	ϕ_{CO_2}	$\phi_{\text{H}_2\text{O}}$	a_{N}	a_{C}
NC	863 (590)	4, 16	0.20	0.34	0.40	0.05	0.01	605	50
	858 (585)	4, 16	0.20	0.34	0.39	0.05	0.02	579	50
	853 (580)	4, 16	0.20	0.34	0.38	0.06	0.02	554	50
	848 (575)	4, 16	0.20	0.34	0.37	0.07	0.02	506	50
	847 (574)	4	0.20	0.34	0.37	0.07	0.02	525	50
	846 (573)	4	0.20	0.34	0.32	0.10	0.03	520	25
		4	0.20	0.34	0.37	0.07	0.02	520	50
	845 (572)	4	0.20	0.34	0.32	0.10	0.03	525	25
		4	0.20	0.34	0.37	0.07	0.02	515	50
	844 (571)	4	0.20	0.34	0.32	0.10	0.04	511	25
		4	0.20	0.34	0.37	0.07	0.02	511	50
	843 (570)	4	0.20	0.34	0.32	0.11	0.04	506	25
		4, 6, 16	0.20	0.34	0.37	0.07	0.02	506	50
	842 (569)	4	0.20	0.34	0.31	0.11	0.04	501	25
		4	0.20	0.34	0.36	0.07	0.02	501	50
	841 (568)	4	0.20	0.34	0.31	0.11	0.04	497	25
		4	0.20	0.34	0.31	0.11	0.04	497	50
	840 (567)	4	0.20	0.34	0.36	0.08	0.02	492	50
	839 (566)	4	0.20	0.34	0.36	0.08	0.02	488	50
	838 (565)	4, 16	0.20	0.34	0.36	0.08	0.02	483	50
	833 (560)	4, 16	0.20	0.34	0.35	0.08	0.02	461	50
	828 (555)	4, 16	0.20	0.34	0.34	0.09	0.03	440	50
	823 (550)	4, 16	0.20	0.34	0.33	0.10	0.03	420	50
N	848–838 (575–565)	4	0.51	0.49				794–725	

summarized in Table II. For a quick overview of the invariant reactions and their temperatures as predicted by the investigated thermodynamic models,^[33–38] a Scheil reaction scheme^[39–41] has been supplied for each model in the supplementary data, using a scaled temperature axis.

III. EXPERIMENTAL

The substrates used for the investigations in the present work were manufactured by casting an Fe-C alloy with a nominal composition corresponding to the eutectoid composition of the Fe-C system (approximately 3.5 at. pct^[54,58]) into ingots of dimensions 80 mm × 30 mm × 10 mm. The ingots were cold-rolled to a thickness of approximately 1 mm. The resulting sheets were cut into rectangular specimens of lateral dimensions of 20 mm × 12 mm and ground and polished (final step 1 μm diamond suspension). The specimens were encapsulated into fused silica tubes containing Ar at a pressure of 2×10⁵ Pa in order to prevent oxidation during the subsequent heat treatment. The specimens were treated at 1273 K (1000 °C, in the γ phase field range) and cooled by putting the fused silica tube on a metallic surface at room temperature. Therefore, a fine pearlitic microstructure with a lamella spacing < 1 μm was achieved.

The pearlitic specimens were nitrided or nitrocarburized in a fused silica tube furnace equipped with mass-flow controllers for the gas supplies of NH₃, H₂, CO, CO₂, H₂O, and CH₄ (the latter not used in the present work).

The composition of the gas atmosphere can be varied precisely in order to control the chemical potentials of N and C in the gas atmosphere recognizing the simultaneous occurrence of several nitriding and carburizing reactions.^[7,59,60] By applying a high flow rate (500 ml min⁻¹), the composition of the gas atmosphere remains constant. In an ideal case, thus, a local equilibrium at the surface of the specimen is achieved. Often, however, a steady state^[10,12,61] prevails at the surface.

The experimental conditions applied in the present work were selected in order to investigate which solid-state equilibria are established at the treatment temperature. Temperatures between 823 K and 863 K (550 °C to 590 °C) were applied. In the most interesting temperature range of 838 K to 848 K (565 °C to 575 °C) (see Section IV), a temperature increment of 1 K was chosen and multiple experiments were performed at each temperature. The temperature was controlled within 1 K. Two different types of atmospheres were chosen, leading to distinctly different types of compound-layer microstructures. The values of the experimental parameters for all experiments, together with the resulting thermodynamic activities of N (reference state N₂ gas at 1×10⁵ Pa) and C (reference state graphite at 1×10⁵ Pa)^[7,59] as calculated using the data for the Gibbs energies of the gaseous species given in Reference 62, are given in Table III. Except for a few cases, a treatment time of 4 hours was applied.

The first experimental series (labeled NC in Table III) was performed using nitrocarburizing atmospheres at temperatures in the range of 838 K to 848 K (565 °C to

Table IV. Microstructure Types (cf. Fig. 4 and Its Discussion) Obtained by Nitrocarburizing of Fe-C Substrates at Different Temperatures

T / K (°C)	Number of Specimens	A	B	C	D	E
848 (575)	3			(x) ^a	x	x
847 (574)	1					x
846 (573)	2				x	x
845 (572)	1				x	x
844 (571)	2			x	x	x
843 (570)	5	(x) ^b	x	x	x	
842 (569)	2		x	x	x	
841 (568)	2	x	x	x		
840 (567)	1	x	x	x		
839 (566)	1	x	x			
838 (565)	3	x	x			

^a1 of 3 specimens
^b2 of 5 specimens.

575 °C) with specific activities of N (400-600) and C (25-50). At 853 K (580 °C), the formation of pure ϵ layers in contact with the pearlitic substrate was observed,^[31] corresponding to the (schematic) diffusion path labeled NC in Figure 3(a). Additional experiments with lower N activities in the temperature range of 838 K to 848 K (565 °C to 575 °C) led to thin, inhomogeneous compound layers that could not be investigated.

The second experimental series (labeled N in Table III) was performed at temperatures in the range of 838 K to 848 K (565 °C to 575 °C) using a pure nitriding atmosphere (NH₃-H₂ mixture), corresponding to N activities between 720 and 800. At 853 K (580 °C), this led to the formation of an $\epsilon/\gamma'/\epsilon$ triple layer on the pearlitic substrates,^[31] corresponding to the diffusion path labeled N in Figure 3(a).

Qualitative phase analysis of the specimens was performed by X-ray diffraction in Bragg-Brentano $\theta-\theta$ geometry, employing a Philips X'Pert MPD equipped with a Co tube and a secondary monochromator, selecting the Co K α radiation. The resulting diffraction patterns were analyzed by Rietveld refinement using the appropriate crystal structure models for all considered phases (see Table I), applying the software TOPAS.^[63] This was done in favor of using the fixed peak position values from databases as, e.g., provided by ICDD that cannot be applied to the ϵ phase which has strongly varying (composition-dependent) values of the lattice parameters.

For light microscopic analysis of the nitrocarburized specimens, cross-sectional samples were prepared by cutting a part from each specimen. This sample was electrolytically coated with Ni in a Watt's bath, to produce a ductile protective layer on top of the brittle compound layer. This sample was then embedded in resin, ground and polished (final stage 1 μ m diamond suspension), and finally etched with 1 pct Nital containing some HCl according to References 23 and 64. The specimens were treated with Groesbeck solution, i.e., an alkaline KMnO₄ solution which stains C-rich phases.^[65] Therefore, the distinction of θ , ϵ , and γ' (in order of decreasing C content) is facilitated. The light microscopic analysis was performed using a ZEISS

Axiophot microscope. In all cases, the presence of phases as recognized in the optical micrographs was verified by analyzing the X-ray diffraction patterns.

IV. RESULTS OF EXPERIMENTAL INVESTIGATION

A. Nitrocarburizing of Fe-C Alloys

The compound layer resulting from nitrocarburizing of the Fe-C alloy at contact with the substrate at $T > 848$ K (575 °C) consists of a pure ϵ layer growing into the $\alpha + \theta$ substrate, corresponding to the schematic diffusion path labeled NC in Figure 3(a). Even after the treatments at 863 K (590 °C), no sign of γ formation was observed. By gaseous nitrocarburizing at $T < 838$ K (565 °C), an $\epsilon/\gamma' + \theta$ double layer growing into the $\alpha + \theta$ substrate is induced, corresponding to the schematic diffusion path labeled NC in Figure 3(c). At intermediate temperatures between 838 K and 848 K (565 °C to 575 °C), transitional microstructures, i.e., in between the two described ones, occur. Thus, the microstructures were classified into five types on the basis of the observations made for increasing nitrocarburizing temperature [from 838 K to 848 K (565 °C to 575 °C)]. Representative examples of all types of microstructures are shown in Figure 4. Type A (Figure 4(a)) refers to the microstructure that *also* occurs below 838 K (565 °C, see above): an ϵ sublayer separated from the substrate by a $\gamma' + \theta$ sublayer. Type B microstructures (Figure 4(b)) show isolated locations where the $\gamma' + \theta$ sublayer becomes penetrated by ϵ grains (see, e.g., the encircled area in Figure 4(b)), which has been pronouncedly realized in type C microstructures (Figure 4(c)), where many ϵ grains are in direct contact with the substrate. In the type D microstructure (Figure 4(d)), the original $\gamma' + \theta$ sublayer then has become a $\gamma' + \epsilon$ sublayer. Finally (see also above), a single-phase ϵ layer results (type E, Figure 4(e)), possibly containing some (retained) γ' and θ "impurities."

In contrast to what is suggested by the above presentation of a transitional series of microstructures of the compound layer, microstructural analysis (in lateral directions) of the whole cross section of the compound layers, obtained by nitrocarburizing at temperatures from 838 K to 848 K (565 °C to 575 °C), revealed that the microstructure of the compound layer, also over the substrate of a single specimen, was often found to vary in lateral directions, i.e., more than one type of microstructure then could be identified in a single compound layer[‡]. Therefore, for each compound

[‡]A section adjacent to the edge of the specimen was ignored due to the possibility of inward diffusion of N and C from more than one side, leading to edge effects.^[12] However, the microstructural transitions present there were compatible with those found in the investigated part of the specimen.

layer, all detected microstructure types were recorded. The results of this analysis are listed in Table IV. Therefore, it becomes clear, despite the microstructural

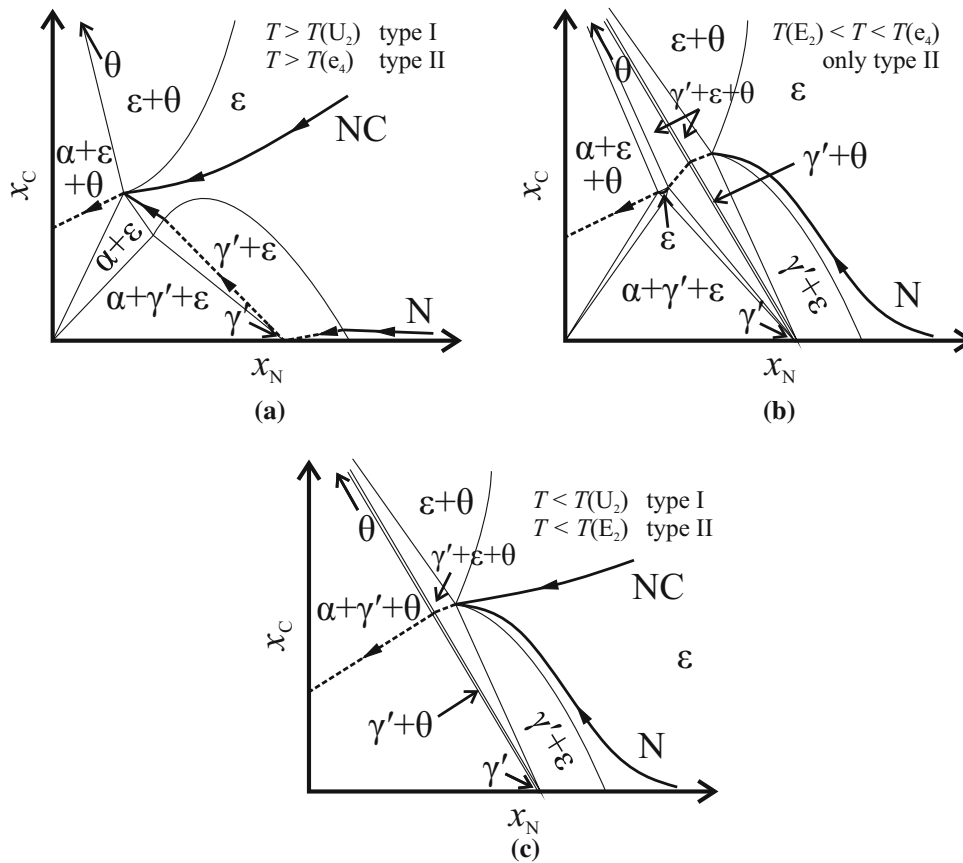


Fig. 3—Schematic diffusion paths superimposed on isothermal sections of the phase diagram of the Fe-N-C system (cf. Fig. 2). Hereby, dashed lines indicate skipping over a two- or three-phase field. (a) Diffusion paths corresponding to the microstructures resulting from nitrocarburizing of the Fe-C alloy above 848 K (575 °C, NC) and nitriding of the Fe-C alloy above 847 K (574 °C, N) superimposed on an isothermal section of the phase diagram at a temperature above the temperature of the U_2 (type I) or e_4 (type II) invariant reaction. (b) Hypothetical, schematic diffusion path corresponding to an $\epsilon/(\gamma' + \theta)/\epsilon$ triple-layer microstructure which is only possible for a type II series of invariant reactions between the temperatures of the e_4 and the E_2 invariant reactions. (c) Diffusion paths corresponding to the microstructure resulting from nitrocarburizing (NC) or nitriding (N) of the Fe-C alloy below 838 K (565 °C) superimposed on an isothermal section of the phase diagram at a temperature below the temperature of the U_2 (type I) or E_2 (type II) invariant reactions.

variation in each compound layer, that starting from lower temperatures and increasing to higher temperatures, the microstructure of the compound layer gradually changes from type A to type E.

B. Nitriding of Fe-C Alloys

In general, the microstructure of the compound layer resulting from nitriding of the Fe-C alloy is much more laterally uniform than that obtained upon nitrocarburizing (see discussion in Section V-A). The compound-layer microstructures after nitriding at 838 K, 841 K, 844 K, and 848 K (565 °C, 568 °C, 571 °C, and 575 °C) are shown in Figure 5. The microstructure obtained upon nitriding at 838 K (565 °C) resembles the type A microstructure resulting from nitrocarburizing of the Fe-C alloy, see Figure 5(a): a (in this case of pure nitriding, more porous) ϵ sublayer is separated from the substrate by a $\gamma' + \theta$ sublayer, corresponding to the diffusion path labeled N in Figure 3(c). In contrast to the nitrocarburizing experiments, only at the temperatures of 840 K (567 °C) and higher single ϵ grains

penetrate the $\gamma' + \theta$ sublayer (Figure 5(b)). The penetration of ϵ into the $\gamma' + \theta$ sublayer at the temperatures of 840 K (567 °C) and higher (cf. Figure 5(b)) appears to be the initiation of the development of a final $\epsilon/\gamma'/\epsilon$ microstructure with a closed γ' sublayer at $T \geq 847$ K (574 °C, Figure 5(d)) in agreement with the results obtained at 853 K (580 °C) in Reference 31, corresponding to the schematic diffusion path labeled N in Figure 3(a). At an intermediate stage, an $\epsilon/(\gamma' + \epsilon)/\epsilon$ compound layer is found (see Figure 5(c)), comparable to the microstructures presented in Reference 21, featuring already a closed ϵ sublayer in contact with the $\alpha + \theta$ substrate.

V. DISCUSSION

A. Development of the Compound-Layer Microstructure Between 823 K and 863 K (550 °C–590 °C)

As an aging phenomenon, the formation of pores in the oldest part of the compound layer, *i.e.*, in the surface-adjacent region,^[7] occurs by decomposition of

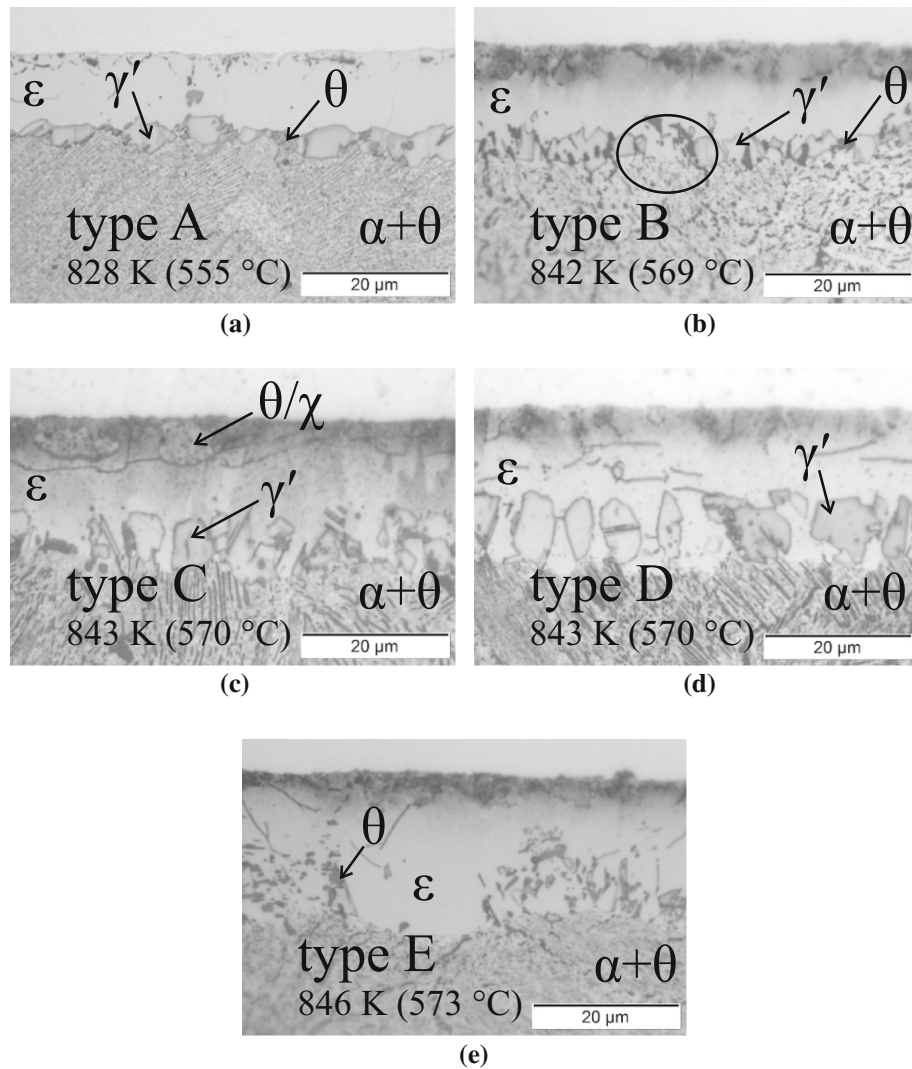


Fig. 4—Micrographs of cross sections showing examples of the typical microstructures occurring upon *nitrocarburizing* between 838 K and 848 K (565 °C to 575 °C). The treatment temperature of the specimens from which the shown examples were taken has been indicated in each micrograph. All specimens were treated for 4 h. (a) ϵ separated from substrate by a $\gamma' + \theta$ sublayer. (b) The $\gamma' + \theta$ sublayer becomes penetrated by ϵ grains at some places, *e.g.*, in the encircled area. (c) γ' , ϵ , and θ in contact with the substrate. (d) ϵ growing around γ' grains, no θ present. (e) ϵ layer, possibly containing γ' and θ impurities.

the metastable ϵ phase into N_2 and/or Fe carbides such as θ or monoclinic χ (Hägg carbide)^[6] and/or the formation of channels and subsequent further reactions with the nitrocarburizing atmosphere.^[25,31,42] This decomposition process needs no further discussion here.

As discussed elsewhere,^[7,12] whereas local solid–solid equilibria can occur at each depth, corresponding to the local gross (laterally averaged) composition, within the compound layer, this may not occur at the gas–solid interface, *i.e.*, at the surface of the compound layer, where moreover at most a stationary state may be established.^[10,61] Then, recognizing that in gaseous nitrocarburizing, as compared to gaseous nitriding, distinctly more reactions participate at the gas/solid interface,^[59,60] it may be understood that the microstructures obtained upon nitriding are more uniform than those obtained upon nitrocarburizing (cf. Sections IV–A and IV–B).

Above the temperature of 848 K (575 °C) for the nitrocarburizing experiments and 844 K (571 °C) for the nitriding experiments, the compound layer contains a continuous ϵ layer (sometimes with small inclusions of γ' and/or θ) in contact with the $\alpha + \theta$ substrate over the whole specimen, see Figures 4(e), 5(d), and Table IV. This is compatible with an $\alpha + \epsilon + \theta$ three-phase equilibrium at the layer/substrate interface. Since the $\alpha + \epsilon + \theta$ three-phase field must be bounded by three two-phase fields, including the $\alpha + \epsilon$ two-phase field, this implies the occurrence of the $\alpha + \epsilon$ equilibrium. These microstructures correspond to the schematic diffusion paths labeled NC (nitrocarburizing) or N (nitriding) in Figure 3(a). They are qualitatively in agreement with the phase diagram resulting from any of the considered models,^[33–38] *i.e.*, at a temperature both (i) above the temperature of the invariant reaction U_2 for type I models and above the temperature of the invariant

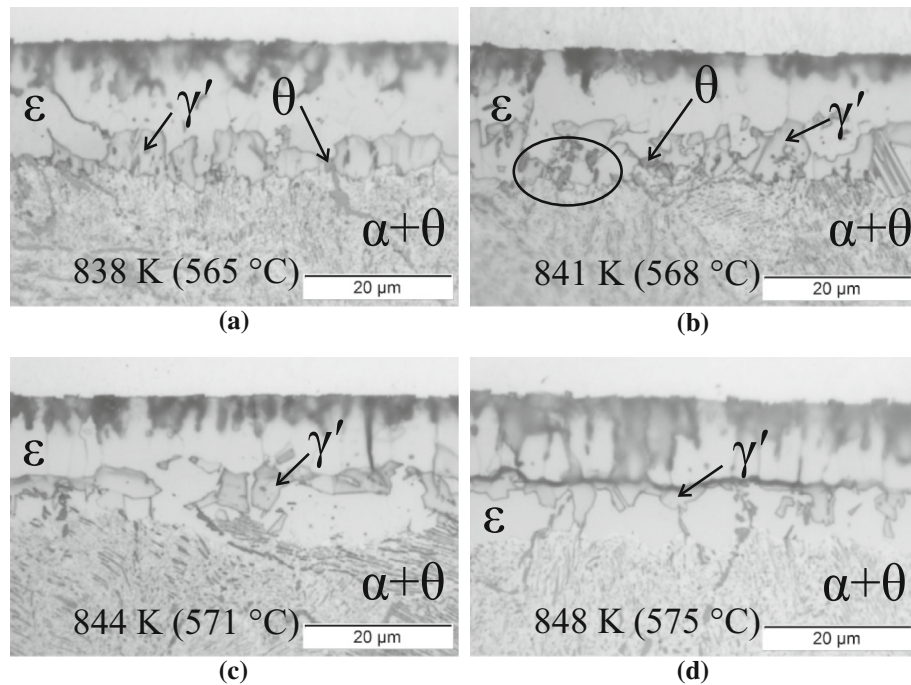


Fig. 5—Micrographs of cross sections showing examples of the typical microstructures resulting from *nitriding* of the Fe-C alloy at 838 K, 841 K, 844 K, and 848 K (565 °C, 568 °C, 571 °C, and 575 °C). (a) Porous ϵ separated from the substrate by a $\gamma' + \theta$ sublayer. (b) The $\gamma' + \theta$ sublayer becomes penetrated by ϵ at some places, e.g., in the encircled area. (c) An $\epsilon/\alpha + \theta$ interface microstructure, showing the establishment of $\alpha + \epsilon$ equilibrium; γ' sublayer forming in the middle of the compound layer. (d) An $\epsilon/\gamma'/\epsilon$ triple-layer microstructure.

reaction e_4 for type II models and (ii), for both types of models, below the temperature of the invariant reaction U_1 . The here observed lowest values of the temperatures at which pure ϵ layers occur on the $\alpha + \theta$ substrate are compatible with the temperatures of the U_2 (type I) or e_4 (type II) reactions of all models from the literature^[33–38] (cf. Table II).

Theoretically, it seems possible that a pure ϵ layer in contact with the $\alpha + \theta$ substrate already occurs at a temperature between the temperature of the E_2 and the e_4 invariant reactions of the type II models; see the second, small triangularly shaped ϵ single-phase field, appearing upon heating through the invariant reaction E_2 (see right part of Figure 2). Then, the concentrations of N and C in the entire ϵ layer must be at least within a compositional triangle connecting pure Fe and the (hypothetical) stoichiometric compounds Fe_4N and Fe_3C , being the upper limits of the homogeneity ranges of the binary γ' and θ phases, respectively. EPMA data collected from ϵ layers growing into Fe-C substrates at 853 K (580 °C), as presented in Reference 31, rule out this possibility: the measured diffusion path starts at high N and C contents and passes through the bottle-neck-shaped area of the phase diagram (see the diffusion path labeled NC in Figure 3(a)), thereby crossing the line connecting the Fe_4N and Fe_3C compositions. Therefore, at least at the temperature of 853 K (580 °C), one large ϵ single-phase field (i.e., not two separate ones as for a type II model between the temperatures of the e_4 and E_2 invariant reactions; see the middle right part of Figure 2) must be present.

The microstructure of the compound layer resulting from nitrocarburizing of Fe-C below 838 K (565 °C) and from nitriding of Fe-C at 838 K (565 °C) consists of an ϵ sublayer separated from the $\alpha + \theta$ substrate by a $\gamma' + \theta$ sublayer in contact with the $\alpha + \theta$ substrate (see Figures 4(a), 5(a), and Table IV). This is compatible with an $\alpha + \gamma' + \theta$ three-phase equilibrium at the layer/substrate interface and, following the same considerations as above, also implies the existence of a $\gamma' + \theta$ two-phase field. This microstructure corresponds to the schematic diffusion path labeled NC in Figure 3(c) and thus is qualitatively in agreement with the phase diagram resulting from any of the investigated models for the system Fe-N-C^[33–38] at a temperature below the temperature of the U_2 invariant reaction (type I model) or the E_2 reaction (type II model), cf. Section I-A and Figures 1 and 2. However, also considering the as-predicted values for the temperatures of these invariant reactions (see Table II), the occurrence of this microstructure at 838 K (565 °C) is only compatible with the model from Reference 38 with a predicted U_2 invariant reaction temperature of 841 K (568 °C) and incompatible with the models from References 33 through 37. Upon cooling, the $\alpha + \epsilon$ equilibrium (see the $\alpha + \epsilon$ two-phase field in the top part of Figure 2) disappears already at higher temperatures than predicted by most of the models from the literature,^[33–37] which is in agreement with earlier findings by our group as presented in Reference 30.

The microstructures of type B, C, and D (cf. Figures 5(b-d) and Table IV) resulting from nitrocarburizing of the Fe-C alloy at the temperatures between

838 K and 848 K (565 °C and 575 °C) are intermediates of type A and type E microstructures. The same holds for the microstructures obtained by nitriding of the Fe-C alloy between 840 K and 844 K (567 °C and 571 °C). Hence, in the temperature range between 840 K and 844 K (567 °C and 571 °C), at the (more or less defined) interface between the compound layer and the substrate four phases (α , γ' , ε , θ) are in contact with each other. However, according to Gibbs' phase rule,^[11,66] an $\alpha + \gamma' + \varepsilon + \theta$ four-phase equilibrium is only possible at a single temperature (and at constant pressure), which here is the temperature of either the invariant reaction U_2 for type I models or the invariant reaction E_2 for type II models (see Figure 2). It is therefore concluded that the microstructures of types B, C, and D represent *nonequilibrium* states. The difficulty of establishing equilibrium so close to the temperature of an invariant reaction is obvious: in that case, the Gibbs energy of the four-phase microstructure differs only slightly from the Gibbs energy of the genuine two-phase or three-phase equilibrium states, and thus the driving force and consequently the transformation rates are vanishingly small. By performing additional experiments in this project, where the specimens were treated overnight, no equilibrium microstructure was established (*i.e.*, microstructures of types B, C, and D occurred with four phases in contact at the compound-layer/substrate interface).

B. The $\alpha + \varepsilon$ Two-Phase Field: Nature of the Invariant Reactions and Their Temperatures

Grains of γ' in contact with θ occur at or below the temperature of 846 K (573 °C) in the nitrocarburized specimens (microstructure type D, for an example see Figure 5(d), cf. Table IV) and at or below the temperature of 844 K (571 °C, see Figure 5(c)) in the nitrided specimens. Assuming local equilibrium at the compound-layer/substrate interface, this is then the highest possible value of the temperature of either the invariant reaction U_2 (type I models) of the invariant reaction e_4 (type II models).

Grains of ε in contact with the $\alpha + \theta$ substrate appear at or above 838 K (565 °C) according to the results from the nitrocarburizing experiments (microstructure type B, for an example see Figure 4(b), cf. Table IV), and at or above 840 K (567 °C) according to the results from the nitrided specimens. On the basis of a similar reasoning as above, this then is the lowest possible value for the temperature of either the U_2 invariant reaction (type I model) or the E_2 invariant reaction (type II model).

The results from the nitriding experiments imply that the invariant reaction(s), U_2 (type I models) or e_4 and E_2 (type II models), leading upon decreasing temperature to the disappearance of the $\alpha + \varepsilon$ equilibrium and the occurrence of the $\gamma' + \theta$ equilibrium, occur within the range of 840 K to 844 K (567 °C to 571 °C). The equivalent temperature range resulting from the nitrocarburizing experiments is larger [838 K to 846 K (565 °C to 573 °C)]. However, in principle, the only few places where ε is in contact with the substrate for the nonequilibrium microstructures of type B (see

Figure 4(b)) and the only few places in which γ' is in contact with the substrate for the nonequilibrium microstructures of type D (see Figure 4(d)) can be considered as kinetic artifacts (see discussion in Section V-A). This leaves the temperatures at which type C microstructures occur as the temperature range in which the invariant reactions U_2 (type I models) or e_4 and E_2 (type II models) occur [840 K to 844 K (567 °C to 571 °C)], see Table IV, confirming the results from the nitriding experiments.

A conclusive proof of a type II series of invariant reactions would be the occurrence of two separate $\gamma' + \varepsilon + \theta$ three-phase equilibria, which is only compatible with the phase diagram for a type II model between the temperatures of the invariant reactions E_2 and e_4 . This could, under the assumption of local equilibrium, be indicated by, *e.g.*, the occurrence of the an $\varepsilon/(\gamma' + \theta)/\varepsilon$ triple-layer microstructure as illustrated by the diffusion path in Figure 3(b): starting in and passing through (full line) the ε single-phase field at high interstitial content, it skips over the first $\gamma' + \varepsilon + \theta$ three-phase field (dashed line), reaching the $\gamma' + \theta$ two-phase field. After passing through the narrow $\gamma' + \theta$ two-phase field (full line), it skips over the second $\gamma' + \varepsilon + \theta$ three-phase field (dashed line), passes through the second ε single-phase field (full line), and finally ends by skipping over the $\alpha + \varepsilon + \theta$ three-phase field (dashed line) to the $\alpha + \theta$ two-phase field (close to the abscissa in Figure 3(b)). Such a microstructure could not be obtained experimentally, as any other conceivable microstructure pointing to exclusively a sequence of invariant reactions of the type II model. Moreover, and as mentioned in Section V-A, under the assumption of local equilibrium, the available EPMA data from specimens treated at 853 K (580 °C) are incompatible with the presence of an isolated second ε single-phase field in the phase diagram at least at that temperature, as would be possible between the temperature of the E_2 and e_4 invariant reactions according to the type II models. On the other hand, the actual concentration values close to the compound-layer/substrate interface, as determined in Reference 31, lie clearly within the already mentioned compositional triangle Fe-Fe₄N-Fe₃C. This could then be explained with a phase diagram of a type II model only a few K above the temperature of the e_4 invariant reaction.

If local equilibrium prevails, the transitional microstructure obtained upon nitriding of the Fe-C alloy at 844 K (571 °C, see Figure 5(c)) also indicates that at this temperature, two isolated ε single-phase fields cannot exist: under local equilibrium conditions, the sublayer morphology $\varepsilon/(\gamma' + \varepsilon)/\varepsilon$ is only possible if the $\gamma' + \theta$ two-phase field in the Fe-N-C phase diagram has already vanished at this lower temperature.

All results in the present work show that it is difficult to reach equilibrium under the applied conditions, especially in the temperature range of 838 K to 848 K (565 °C to 575 °C) in which transitional microstructures occurred, clearly deviating from equilibrium. In general, also if a microstructure complies with Gibbs' phase rule, an equilibrium state is therefore not proven. Thus, the above observations pointing toward either a type I or

type II series of invariant reactions could also be explained by kinetic effects.

Thermodynamics can predict a sharp transition from microstructures in which α is in contact with ε at higher temperature to microstructures in which γ' is in contact with θ at lower temperature (in this work at the compound-layer/substrate interface). This means a transition at a single temperature *via* the U_2 invariant reaction (type I model) or *via* invariant reactions at two temperatures, *i.e.*, the e_4 and E_2 (type II model) invariant reactions. In reality, due to kinetic limitations (see above), this transition occurs gradually over a narrow range of temperatures: approaching an invariant temperature, the driving force for the transition is very small, becoming nil at the invariant temperature.

In view of the results obtained in this work and the above discussion, it is not possible to draw unambiguously a final conclusion which of both types of models better describes the physical reality. In case of a type I model as predicted by References 33, 35, 36 and 38, the temperature of the invariant reaction U_2 , $\alpha + \varepsilon \rightleftharpoons \gamma' + \theta$, can be given as $842 \text{ K} \pm 2 \text{ K}$ ($569 \text{ }^\circ\text{C} \pm 2 \text{ }^\circ\text{C}$); in case of a type II model as predicted by References 34 and 37, the reactions e_4 and E_2 must occur subsequently within the temperature range from 840 K to 844 K ($567 \text{ }^\circ\text{C}$ to $571 \text{ }^\circ\text{C}$).

All microstructures that emerged as a result of the nitriding and nitrocarburizing treatments performed in the present work are compatible with the observations of Reference 30. However, in the present work, the $\alpha + \varepsilon$ equilibrium was not clearly established at 843 K ($570 \text{ }^\circ\text{C}$) as in Reference 30, but at a slightly higher temperature: the temperature of the U_2 invariant reaction as determined in the present work (if a type I model is assumed), and as due to smaller steps in temperature in the performed series of experiments, is close to the higher end of the temperature range of 833 K to 843 K ($560 \text{ }^\circ\text{C}$ to $570 \text{ }^\circ\text{C}$) as proposed for the U_2 reaction in Reference 30.

C. Compatibility of Experimental Data with the Models from the Literature

The temperatures of the invariant reactions as calculated in the present work by the application of the models for the Fe-N-C system given in the literature^[33–38] are listed in Table II. Experimentally determined data from recent works^[32,61] and the temperature of the invariant reaction U_2 (if a type I model is assumed) or the temperature range for the invariant reactions E_2 and e_4 (if a type II model is assumed) as determined in the present work are given in Table II. Matches of the experimental and calculated data have been marked with an asterisk.

Considering the temperatures of the invariant reactions in the binary Fe-N system (c , e_2 , and e_3), all models except the model of Reference 38 give an acceptable but varying degree of agreement with the experimentally determined data.

The temperature of the ternary invariant reaction E_1 (cf. Figure 1) is also reproduced accurately by most^[33,34,36,37] models. For the invariant reaction U_1 ,

only the model of Reference 36 gives a value which is close to the experimentally determined range.^[32] Strikingly, the values predicted by the models of References 34 and 37 are almost 100 K higher than the experimental value reported in Reference 32. The other models^[33,35,38] give a too low value, disagreeing with both the results from the present work and from Reference 32.

The temperature of the invariant reaction U_2 that was determined experimentally in the present work is only reproduced well by the model of Reference 38. For all other invariant temperatures in the ternary system, however, this model^[38] gives inaccurate values. The values for the temperature of the invariant reaction U_2 as calculated using the models of References 33 and 35 are about 20 K too low. The model from Reference 36 gives a value which is much too low in view of the here determined experimental result. Also note that the type II models^[34,37] give a slightly too low temperature range for the transition between the $\gamma' + \theta$ and the $\alpha + \varepsilon$ equilibria (reactions e_4 and E_2).

Considering all invariant reactions in the system Fe-N-C, the model from Reference 36 agrees best with the experimental data, but note the huge discrepancy with the experimental value for the invariant reaction U_2 (see above). The model from Reference 37 also gives an overall good agreement with the experimental data for the invariant temperatures if a type II model is assumed. Moreover, it has already been shown by our group that the model from Reference 37 agrees better with the experimental data for phase boundaries^[12,32] and the thermodynamics of the ε phase.^[31,67]

The above evaluation suggests that the development of a new model for the system Fe-N-C is timely. Such a model must yield a good agreement with the experimental data pertaining to the invariant temperatures, the phase boundaries, and the thermodynamics of especially the ε phase.

VI. CONCLUSIONS

1. Inspection of all models for the Fe-N-C system available in the literature indicates two different possibilities for the (series of) invariant reaction(s) leading to the transition from the $\alpha + \varepsilon$ two-phase field in the Fe-N-C system at higher temperatures to the $\gamma' + \theta$ two-phase field at lower temperatures. Models of type I realize this transition *via* the invariant reaction $\alpha + \varepsilon \rightleftharpoons \gamma' + \theta$ (U_2). Models of type II realize this transition *via* the invariant reactions $\varepsilon \rightleftharpoons \gamma' + \theta$ (e_4) and $\varepsilon \rightleftharpoons \alpha + \gamma' + \theta$ (E_2).
2. Microstructural analyses of the compound layer developing on Fe-C substrates upon nitriding and nitrocarburizing for a series of temperatures showed that both types of models are qualitatively compatible with the experimental results. A sharp transition from the $\alpha + \varepsilon$ to the $\gamma' + \theta$ equilibrium upon cooling is not found due to kinetic reasons.
3. The minimum temperature at which the $\alpha + \varepsilon$ equilibrium of the Fe-N-C system is established

has been determined at 844 K (571 °C). The maximum temperature at which the $\gamma' + \theta$ equilibrium is established has been determined at 840 K (567 °C). This corresponds to a temperature of the invariant reaction U_2 of 842 K \pm 2 K (569 °C \pm 2 °C) if a type I model is assumed and a temperature range of 844 K to 840 K (567 °C to 571 °C) in which upon cooling the e_4 and E_2 invariant reactions must occur subsequently according to a type II model.

- Comparison of the available experimental data of temperatures of the invariant reactions and the phase boundaries with the predictions calculated by applying models presented in the literature shows that none of the published models provide a satisfactory description of the experimental data. A remodeling of the Fe-N-C system is required.

ACKNOWLEDGMENTS

Open access funding provided by Max Planck Society. The authors are very grateful to Dr. B. Hallstedt, RWTH Aachen, Germany, for assistance with formulating the models from References 34 and 37 in terms of the compound-energy formalism and implementing them into a Thermo-Calc database, and also for supplying Thermo-Calc databases for the thermodynamic descriptions given in References 35 and 36.

OPEN ACCESS

This article is distributed under the terms of the Creative Commons Attribution 4.0 International License (<http://creativecommons.org/licenses/by/4.0/>), which permits unrestricted use, distribution, and reproduction in any medium, provided you give appropriate credit to the original author(s) and the source, provide a link to the Creative Commons license, and indicate if changes were made.

ELECTRONIC SUPPLEMENTARY MATERIAL

The online version of this article (doi:10.1007/s11661-016-3605-5) contains supplementary material, which is available to authorized users.

REFERENCES

- K.H. Jack: *Proc. R. Soc. London, Ser. A*, 1948, vol. 185, pp. 41–55.
- F.K. Naumann and G. Langenscheid: *Arch. Eisenhüttenwes.*, 1965, vol. 36, pp. 677–82.
- V. Raghavan: *Trans. Indian Inst. Met.*, 1984, vol. 37, pp. 293–301.
- V. Raghavan: *Phase Diagrams of Ternary Iron Alloys*, ASM International, New Delhi, 1987, pp. 153–65.
- V. Raghavan: *J. Phase Equilib.*, 1993, vol. 14, pp. 620–21.
- D.H. Jack and K.H. Jack: *Mater. Sci. Eng.*, 1973, vol. 11, pp. 1–27.
- E.J. Mittemeijer: *ASM Handbook, Volume 4A, Steel Heat Treating Fundamentals and Processes*, chap. Fundamentals of Nitriding and Nitrocarburizing, ASM International, 2013, pp. 619–46.
- H.A. Wriedt, N.A. Gokcen, and R.H. Nafziger: *J. Phase Equilib.*, 1987, vol. 8, pp. 355–77.
- H. Okamoto: *J. Phase Equilib.*, 1992, vol. 13, pp. 543–65.
- E.J. Mittemeijer, M.A.J. Somers, eds.: *Thermochemical Surface Engineering of Steels*, Woodhead Publishing, Cambridge, 2015.
- E.J. Mittemeijer: *Fundamentals of Materials Science*, Springer, Heidelberg, 2011.
- T. Woehrl, A. Leineweber, and E.J. Mittemeijer: *Metall. Mater. Trans. A*, 2012, vol. 43A, pp. 2401–13.
- J.S. Kirkaldy and D.J. Young: *Diffusion in the Condensed State*, The Institute of Metals, London, 1987.
- F.J.J. van Loo: *Prog. Solid State Chem.*, 1990, vol. 20, pp. 47–99.
- A.A. Kodentsov, G.F. Bastin, and F.J.J. van Loo: *J. Alloys Compd.*, 2001, vol. 320, pp. 207–17.
- M. Kizilyalli, J. Corish, and R. Metselaar: *Pure Appl. Chem.*, 1999, vol. 71, pp. 1307–25.
- E. Scheil, W. Mayr, and J. Müller: *Arch. Eisenhüttenwes.*, 1962, vol. 33, pp. 385–92.
- D. Gerardin, H. Michel, J.P. Morniroli, and M. Gantois: *Mem. Sci. Rev. Metall.*, 1977, vol. 74, pp. 457–67.
- J. Matauschek and H. Trenkler: *Härt.-Tech. Mitt.*, 1977, vol. 32, pp. 177–81.
- E.J. Mittemeijer, W.T.M. Straver, P.F. Colijn, P.J. van der Schaaf, and J.A. van der Hoeven: *Scr. Metall.*, 1980, vol. 14, pp. 1189–92.
- A. Wells and T. Bell: *Heat Treat. Met.*, 1983, vol. 10, pp. 39–44.
- H.C.F. Rozendaal, F. Colijn, and E.J. Mittemeijer: *Surf. Eng.*, 1985, vol. 1, pp. 30–42.
- A. Wells: *J. Mater. Sci.*, 1985, vol. 20, pp. 2439–45.
- A. Wells: *Thin Solid Films*, 1985, vol. 128, pp. L33–36.
- M.A.J. Somers and E.J. Mittemeijer: *Surf. Eng.*, 1987, vol. 3, pp. 123–37.
- X. Zuyao and L. Lin: *Mater. Sci. Technol.*, 1987, vol. 3, pp. 325–28.
- M.A.J. Somers, P.F. Colijn, W.G. Sloof, and E.J. Mittemeijer: *Z. Metallkd.*, 1990, vol. 81, pp. 33–43.
- S. Pietzsch, S. Bohmer, and H.-J. Spies: *Proc. 2nd Int. Conf. Carburizing and Nitriding with Atmospheres*, 1995, pp. 295–300.
- H. Du, M.A.J. Somers, and J. Ågren: *Metall. Mater. Trans. A*, 2000, vol. 31A, pp. 195–211.
- M. Nikolussi, A. Leineweber, E. Bischoff, and E.J. Mittemeijer: *Int. J. Mater. Res. (formerly Z. Metallkd.)*, 2007, vol. 98, pp. 1086–92.
- H. Göhring, A. Leineweber, and E.J. Mittemeijer: *Metall. Mater. Trans. A*, 2015, vol. 46A, pp. 3612–26.
- T. Woehrl, H. Cinaroglu, A. Leineweber, and E.J. Mittemeijer: *Int. J. Mater. Res. (formerly Z. Metallkd.)*, 2016, vol. 107, p. 191.
- J. Slycke, L. Sproge, and J. Ågren: *Scand. J. Metall.*, 1988, vol. 17, pp. 122–26.
- J. Kunze: *Nitrogen and Carbon in Iron and Steel: Thermodynamics*, Akademie-Verlag, Berlin, 1990.
- H. Du and M. Hillert: *Z. Metallkd.*, 1991, vol. 82, pp. 310–16.
- H. Du: *J. Phase Equilib.*, 1993, vol. 14, pp. 682–93.
- J. Kunze: *Härt.-Tech. Mitt.*, 1996, vol. 51, pp. 348–55.
- P. Franke and H.J. Seifert (eds.): *Landolt-Börnstein - Group IV Physical Chemistry, Volume 19C1 - Thermodynamic Properties of Inorganic Materials compiled by SGTE. Ternary Steel Systems: Phase Diagrams and Phase Transition Data*, Springer, 2012.
- E. Scheil: *Arch. Eisenhüttenwes.*, 1936, vol. 9, pp. 571–73.
- H.L. Lukas, E.-T. Henig, and G. Petzow: *Z. Metallkd.*, 1986, vol. 77, pp. 360–67.
- B. Predel, M. Hoch, and M. Pool: *Phase Diagrams and Heterogeneous Equilibria*, Springer, Berlin, 2004.
- H. Göhring, S. Kante, A. Leineweber, and E.J. Mittemeijer: *Int. J. Mater. Res. (formerly Z. Metallkd.)*, 2016, vol. 107, pp. 203–16.
- A. Prince: *Alloy Phase Equilibria*, Elsevier Publishing Company, Amsterdam, 1966.
- H. Lukas, S.G. Fries, and B. Sundman: *Computational Thermodynamics—The Calphad Method*, Cambridge University Press, Cambridge, 2007.
- S. Hertzman: *Metall. Trans. A*, 1987, vol. 18, pp. 1753–66.
- M. Hillert and L.-I. Staffansson: *Acta Chem. Scand.*, 1970, vol. 24, pp. 3618–26.

47. B. Sundman and J. Ågren: *J. Phys. Chem. Solids*, 1981, vol. 42, pp. 297–301.
48. M. Hillert: *J. Alloys Compd.*, 2001, vol. 320, pp. 161–76.
49. O. Redlich and A.T. Kister: *Ind. Eng. Chem.*, 1948, vol. 40, pp. 345–48.
50. J. Ågren: *Metall. Trans. A*, 1979, vol. 10A, pp. 1847–52.
51. J. Kunze: *Steel Res.*, 1986, vol. 57, pp. 361–67.
52. K. Frisk: *CALPHAD*, 1987, vol. 11, pp. 127–34.
53. K. Frisk: *CALPHAD*, 1991, vol. 15, pp. 79–106.
54. P. Gustafson: *Scand. J. Metall.*, 1985, vol. 14, pp. 259–67.
55. B. Uhrenius and H. Harvig: *Met. Sci.*, 1975, vol. 9, pp. 67–82.
56. M. Jarl: *Scand. J. Metall.*, 1978, vol. 7, pp. 93–101.
57. J.-O. Andersson, T. Helander, L. Höglund, P. Shi, and B. Sundman: *CALPHAD*, 2002, vol. 26, pp. 273–312.
58. H. Göhring, A. Leineweber, and E.J. Mittemeijer: *CALPHAD*, 2016, vol. 52, pp. 38–46.
59. A. Leineweber, T. Gressmann, and E.J. Mittemeijer: *Surf. Coat. Technol.*, 2012, vol. 206, pp. 2780–91.
60. E.J. Mittemeijer and J.T. Slycke: *Surf. Eng.*, 1996, vol. 12, pp. 152–62.
61. J. Stein, R.E. Schacherl, M.S. Jung, S. Meka, B. Rheingans, and E.J. Mittemeijer: *Int. J. Mater. Res. (formerly Z. Metallkd.)*, 2013, vol. 104, pp. 1053–65.
62. M.W. Chase, Jr.: NIST-JANAF Thermochemical Tables, Fourth Edition, *J. Phys. Chem. Ref. Data Monogr.*, 1998, vol. 9, p. 1.
63. A.A. Coelho: *Topas*, Bruker AXS GmbH, Karlsruhe, 2003.
64. P.F. Colijn, E.J. Mittemeijer, and H.C.F. Rozendaal: *Z. Metallkd.*, 1983, vol. 74, pp. 620–27.
65. G. Petzow: *Metallographic Etching: Techniques for Metallography, Ceramography, Plastography*, ASM International, Materials Park, 1999.
66. M. Hillert: *Phase Equilibria, Phase Diagrams, and Phase Transformations: Their Thermodynamic Basis*, Cambridge University Press, Cambridge, 1998.
67. T. Woehrlé, A. Leineweber, and E.J. Mittemeijer: *Metall. Mater. Trans. A*, 2013, vol. 44A, pp. 2548–62.